Optimization of Gas Sensors Measurements by Dynamic Headspace Analysis Supported by Simultaneous Direct Injection Mass Spectrometry

Luigi Quercia[1,2], Iuliia Khomenko[3], Rosamaria Capuano[1], Matteo Tonezzer[3,4,5], Roberto Paolesse[6], Alexandro Catini[1], Franco Biasioli[3], Corrado Di Natale[1]

1. Department of Electronic Engineering, University of Rome Tor Vergata, Via del Politecnico, 00133 Roma; Italy
2. ENEA, Centro Ricerche Casaccia, Via Anguillarese 301, 00123; Roma; Italy
3. Department of Food Quality and Nutrition, Research and Innovation Centre, Fondazione Edmund Mach, 38010, San Michele all' Adige, TN, Italy
4. IMEM-CNR, Sede di Trento-FBK, Via alla Cascata 56/C, 38123 Povo-Trento, Italy
5. Center Agriculture Food Environment, University of Trento/Fondazione Edmund Mach, via E. Mach 1, 38010 San Michele all'Adige, Italy
6. Department of Chemical Science and Technology, University of Rome Tor Vergata via della Ricerca Scientifica 00133 Roma; Italy

Corresponding Authors

Prof. Corrado Di Natale

Department of Electronic Engineering; University of Rome Tor Vergata

Via del Politecnico, 00133 Roma; Italy

dinatale@uniroma2.it

Abstract

Dynamic headspace extraction is frequently used in gas sensors measurements. Although the distortion of headspace composition is a possible artefact, its influence in sensors signals interpretation has not been deeply studied. In this paper, taking advantage of the on-line combination of a quartz microbalance gas sensor array with a proton transfer reaction mass spectrometer, we have been able to track the evolution of the concentration of volatile compounds along 60 seconds of extraction of the headspace of differently treated tomato paste.

An electric equivalent circuit model of the dynamic headspace sampling has been introduced. Proton transfer reaction mass spectrometer signals show that VOCs are characterized by a large diversity of the evolution of the concentration in the sensors cell.

Sensors signals do not follow the concentration of volatile compounds but they grow approaching a steady value. The contrasting behaviour between sensors and the concentration of most of VOCs is explained considering that water is the dominant component in the tomato paste sample and that water is one of those compounds whose concentration in the sensor cell steadily grows. Analysis of variance demonstrates that in this experiment the largest separation between classes occurs when the concentration of compounds in the sensor cell reached its peak. Thus, although the sensor signals continue to rise, the information content of the signals decay. This finding suggests that measurement protocols need to be adjusted according to the properties of the

sample and that the actual measurement time could be much shorter than predicted from the behaviour of sensor signal and typically used.

Keywords: Dynamic Headspace; Quartz microbalance; Porphyrins; Proton Transfer Reaction Mass Spectrometry

Introduction

The optimization of measurement protocols is a preeminent element of gas sensors applications. However, in spite of this evident importance, topics such as sample conditioning and uptake are seldom investigated. In most of the cases, procedures previously optimized for analytical methods, such as gas-chromatography and mass spectrometry, are uncritically transferred to gas sensors with little consideration of the peculiar properties of these devices [1].

The standard arrangement of sensors in closed cells requires the transfer of the gaseous sample typically mixed with a carrier gas. In case of liquid or solid samples, the measurement procedure is typically based on dynamic headspace extraction. This method is directly derived by gas-chromatography practice where samples (either liquid or solid) are enclosed in sealed vials endowed with a pierceable septum [2]. Vials are kept at constant temperature in order to establish the equilibrium composition of the headspace; then, the headspace is sampled by a flow of a carrier gas (typically N_2) and transferred to the sensors cell. The extraction of the headspace disrupts the equilibrium between gas and liquid/solid phase and a competition between the extraction of volatile compounds and the evaporation of molecules occurs after the extraction of the first quota of volatile molecules.

In gas-chromatography the injected volumes are small and the extraction time is short, thus it is reasonable to assume that it does not affect the actual concentration of volatile compounds [3]. On the other hand, the response times of sensors are usually longer and the perturbation of the headspace composition cannot be neglected.

Most of the attention in the past literature has been given to the reproducibility of sample extraction methods [1]. This is a very important concern: although nominally similar, differently extracted samples are likely to be perceived by the sensors as belonging to distinct classes. In comparison, one of the most striking properties of natural olfaction is the capability to identify samples disregarding the modality in which the odour occurs, and it is common experience that odours can be identified even against variable background or at variable concentration [4]. Artificial olfaction systems are still quite distant from this abstraction capability; rather, sensors provide signals linked to sample composition. Furthermore, in complex matrices the evaporation enthalpies proper of each compound, combined with the effects of non-ideal behaviour of real mixtures, make the modification of headspace unpredictable.

In this paper, the effects of sampling time on sensors response have been investigated and a three-class experiment has been designed. The experiment was aimed at classifying samples in three classes of tomato paste: pristine, inoculated with *Penicillium expansum* then stored at 8°C for one week, and inoculated with *Penicillium expansum* stored for one week at 8°C under exposure to vapours of thyme essential oil. Thyme essential oil is known to inhibit the growth of microorganisms and thus to protect food from spoilage [5,6]. Beside their intrinsic potential interest, the three groups of samples are supposed to be sufficiently different to

provide the basis to study the influence of measurement time and the evolution of volatile compounds during the direct headspace extraction.

Gaseous samples were analysed by an array of quartz microbalances coated with porphyrinoids [7] connected in series with a Proton Transfer Reaction Time of Flight Mass Spectrometer (PTR-ToF-MS) [8].

Such a setup enables the simultaneous measurement of the same sample with both techniques. The combination of electronic nose and PTR-ToF-MS has been recently demonstrated to be an effective methodology to study complex mixtures such as the culture media of red blood cells infected with *plasmodium falciparum* [9].

Results show that the concentration of volatile organic compounds (VOCs) in the headspace quickly reaches a peak followed by a progressive depletion of compounds in the carrier. The interpretation of signals has been corroborated by an equivalent circuit model of dynamic headspace sampling which shows that the ratio between the speed of filling of sensor cell and the rate of the evaporation of the VOC is crucial to determine the behaviour of concentration of VOCs. The use of equivalent circuits to describe sensor responses has been recently demonstrated in case of Langmuir isotherm adsorption [10].

However, due to the abundance of water vapour and the non-negligible sensitivity of sensors to humidity, the variation of VOCs content is not immediately visible in sensor signals. Here it is shown that, in spite of the progressive increase of sensor signal that demonstrates an accumulation of molecules onto the sensor surface, the information content measured by variance analysis shows a synchronous peak with the VOCs content in the headspace. Tomato paste inoculated/not-inoculated with a common spoiling microorganism and treated/non-treated with thyme oil as possible inhibitor has been chosen as relevant case study.

These results provide an input to the design of gas sensors arrays in experiments where dynamic headspace extraction is used.

Materials and methods

Tomato paste samples

Samples were prepared from commercial tomato paste, same brand bought over the counter. Samples were inoculated with *Penicillium expansum* (10^6 UFC/ml) and stored at 8°C for a week. A part of samples was exposed to a proper concentration of vapours of essential oil of thyme (*Thymus vulgaris*) during the storage, with the aim of inhibiting the fungus growth. After one week storage at 8°C, the inhibition effect of thyme vapour was verified by visual inspection and confirmed by microbiological measurements: inoculated samples showed between 4 and 5 times the original fungal load while samples stored under thyme vapours had only between two and three times the original fungal load [7]. Eventually three groups of samples were prepared: pristine tomato paste, inoculated tomato paste and inoculated tomato paste stored under thyme oil vapours. Ten samples were prepared for each group, to be analysed simultaneously by e-nose and PTR-ToF-MS.

Headspace analysis

Samples were handled by a multipurpose GC automatic sampler (Autosampler, Gerstel GmbH, Mulheim am Ruhr, Germany). Headspace VOCs from the samples were delivered by a nitrogen carrier to the gas sensors measurement cell and to the PTR-ToF-MS connected in series. VOC measurements were performed in 20 mL vials. Samples were stored at 4°C then, before analysis, they were incubated for 30 min at 37°C and measured for 70 s in direct mode. A constant flow of 150 sccm of zero air produced by the gas calibration unit (Ionicon

Analytik GmbH, Innsbruck, Austria) was applied for the dilution of the headspace and preventing the memory effects between measurements.

Proton Transfer Reaction Mass Spectrometry

The headspace of tomato paste samples was analysed by direct injection in a PTR-ToF-MS 8000 apparatus (Ionicon Analytik GmbH, Innsbruck, Austria) after passing a Gas Sensor Array. The instrumental conditions in the drift tube were as follows: drift voltage 538 V, drift temperature 110°C, drift pressure 2.80 mbar, producing a reduced electric field E/N=130 Td (1 Td = 10^{-17} Vcm^2), where E is the electric field and N is the gas number density (molecules/cm^3). In order to increase the sensitivity, an ion funnel was operated at the end of the drift tube [11]. The sampling time per channel of ToF acquisition was 0.1 ns, amounting to 350,000 channels for a mass spectrum ranging up to m/z = 350. Every single spectrum is the sum of 30030 acquisitions lasting 33 μs each, resulting in a time resolution of 1 s.

Sensor Array

The gas sensor array was an ensemble of six quartz microbalances (QMB). In these sensors, a mass change (Δm) on the quartz surface results in a frequency change (Δf) of the electrical output signal of an oscillator circuit at which each sensor is connected. In the low-perturbation regime, Δm and Δf are linearly proportional [12]. QMBs had a fundamental frequency of 20 MHz, corresponding to a mass resolution of the order of a few nanograms. The six sensors were functionalized with molecular films of 5,10,15,20-tetrakis-(4-butyloxyphenyl)porphyrins, but differentiated by the metal complexed at the molecular core: copper, cobalt, zinc, magnesium, manganese chloride, and iron chloride. Metalloporphyrins were synthesized following literature methods [13].

The sensors were used with an in-house designed and manufactured sensor system where the gas sensors are complemented by temperature and relative humidity sensors. Each QMB is connected to an oscillator circuit, and the frequency of the oscillators outputs are measured respect to a temperature compensated reference quartz that allows for a frequency resolution of 0.1 Hz. Digital electronics is implemented in a Field Programmable Gate Array. A single USB connection provides both the power supply and the data connection. Functions and data acquisition are controlled with a software running in Matlab.

Data processing and statistical analysis

Data processing of PTR-ToF-MS spectra included dead time correction, external calibration and peak extraction steps performed according to a procedure described elsewhere [14]. The baseline of the mass spectra was removed after averaging the whole measurement, and peak detection and peak area extraction were performed by using a modified Gaussian to fit the data [15]. To determine the concentrations of volatile compounds in ppbv (part per billion by volume) the formulas described by Lindinger et al. [16] were used assuming a constant reaction rate coefficient ($k=2\times10^{-9}$ cm^3/s) for H_3O^+ as primary ion.

The statistical significance of PTR-MS peaks and sensors signals was evaluated with the non-parametric Kruskal-Wallis rank sum test followed by Bonferroni correction in case of multiple comparisons.

Variance analysis and multivariate analysis were performed in Matlab R2020a.

Results and discussion.

Ten samples for each of three classes (pristine tomato paste, inoculated tomato paste, and inoculated tomato paste treated with thyme oil) were closed in vials. Measurements were taken with an autosampler keeping the sample at the constant temperature of 40°C and using nitrogen as gas carrier.

The headspace was sampled for 70 s and delivered to the electronic nose and the PTR connected in series.

In dynamic sampling the headspace of a vial containing the sample is extracted by a carrier flow and transferred into a cell where the detector, either sensors or mass spectrometer injector, are placed. During the transfer, the concentration in the vial is diluted by the carrier flow. The time behaviour of the VOCs concentration in the sensor cell depends on several factors including the evaporation of VOCs inside the vial, the dilution of the headspace in the carrier and the filling of the sensor cell. The whole process can be adequately represented by a RC circuit made of three blocks, each representing one of the factors previously mentioned. The model is shown in Figure 1. The capacitors in the circuit represent the volumes of vial and sensor cell, the voltage is the saturation pressure of the volatile compound and the resistors define the transfer of molecules into the different compartments. The complete and detailed analysis of circuit in Figure 1A and the dimensioning of circuit elements to the real case are out of the scope of this paper. Here we are interested to qualitatively study the behaviour of the output voltage which represents the pressure of the VOC in the chamber. The shape of the dynamic concentration at which sensors and PTR are exposed depends on the balance between the three above mentioned processes. Carrier flow and sensor cell filling are maintained constant, while the evaporation rate of different VOCs may be extremely variable. To study the different time evolution of VOCs, we calculated V_{cell} at different ratio between the time constant of sensor chamber filling (R_{cell}*C_{cell}) and the time constant of headspace formation (R_{evap}*C_{vial}). The carrier is activated, closing the switch, only after the charge of C_{vial} is completed. In practice, it corresponds to start the measure of the headspace after the headspace reached the equilibrium condition. The circuit in figure 1A was simulated in MATLAB 2020b/Simscape Electrical environment.

Figure 1B shows the behaviour of V_{cell} for different ratio of time constants. When the cell filling is faster than the evaporation rate, the behaviour is non-linear characterized by an overshoot. On the other hand, when the evaporation rate is faster than the filling of the cell the concentration at which sensors are exposed, it grows progressively.

In a mixture of compounds, such as in the tomato paste, we expect a diversity of behaviours.

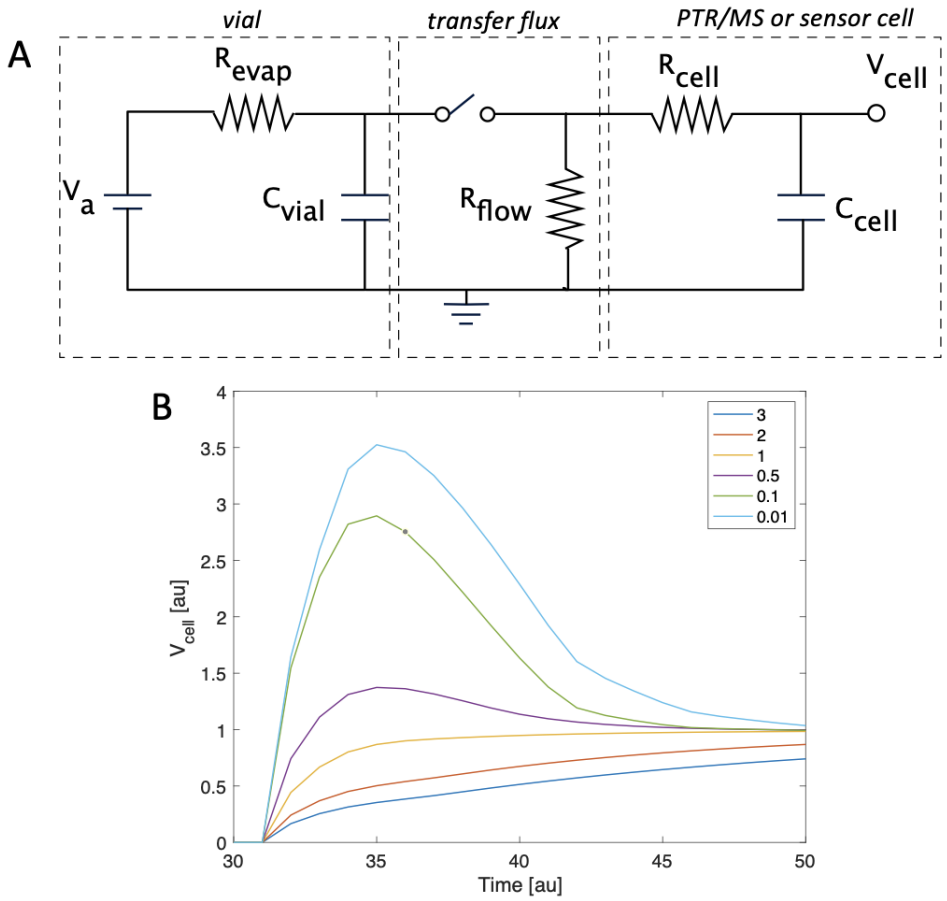

*Figure 1: A: electric equivalent model of the evolution of volatile compounds in a sensor (or detector) cell. B: output voltage, representing the concentration in the sensor's cell, as a function of the time constant ratio between the sensor cell filling (R_{cell}*C_{cell}) and the time constant of headspace formation (R_{evapl}*C_{vial}). (metterei nome e unità nella legenda)*

The real time response of PTR-ToF-MS data gives the chance to better study the evolution of the concentration of compounds in the sensors or the detector cell. PTR-ToF-MS detected 131 different peaks. For each peak the average in the 30 measurements was evaluated. To understand the different time behaviour of the peaks, the time evolution has been clustered by a k-means algorithm in 6 classes. For the scope we were interested to study the shape of the signal evolution. The time evolution of the 131 peaks was analyzed with principal component analysis to evidence the differences between the peaks. Figure 2 shows the scores plot of the PCA. For each group the peaks signal evolution is also shown. To focus the attention on the shape of the behaviour, the peaks signals was normalized in the [0-1] interval.

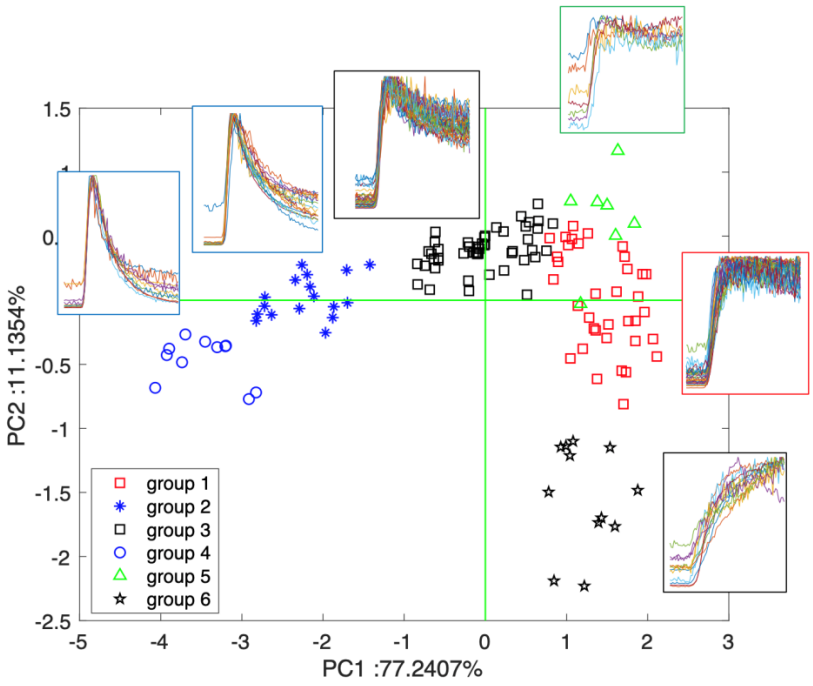

Figure 2: PCA of peaks time evolution reveals the different time constant of evaporation process of the different VOCs. Groups have been defined by k-means…etc (see text)

2

Sensors signals on the other hand do not show the behaviour of PTR-ToF-MS peaks. Figure 3 shows the sensors signals recorded during the exposure to all samples. The signals are scaled for the frequency at the time of sample injection, so the frequency shift to the adsorption of molecules in the sample is considered.

Sensors signals are rather reproducible, and considering the working mechanism of quartz microbalances, the sensors signals suggest a progressive increase of the amount of absorbed molecules. The end of exposure and the beginning of cleaning with a stream of technical air is also visible in Figure 3 and it shows a prompt start of the desorption process.

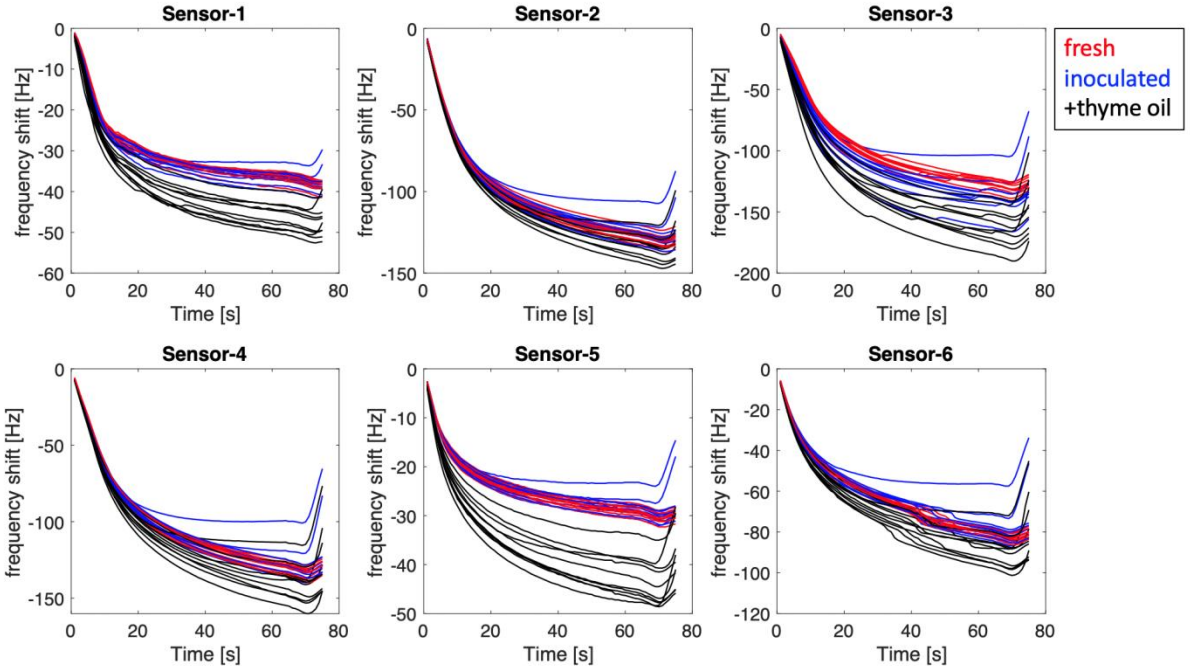

Figure 3: Evolution of sensors signals during the exposure to samples. In each plot the signals of the same sensor are compared. A certain tendency to separate the three classes can be observed. Samples treated with thyme oil show higher signals which make them clearly identifiable respect to the other two classes.

In this experiment we were interested in studying the variation in the information content of the sensor signal during the exposure. The interpretation of adsorption processes suggests that the information of sensor signal increases during the exposure to the sample. Indeed, the behaviour of sensors in figure 3 shows a progressive increase of the signals and an apparent increase of the differences between classes. This is immediately perceived for class 3 (samples added with thyme oil), while the differences between the other two classes are less recognizable from a visual comparison of the signals.

Sensors signals seem to be more influenced by the compounds lying in the right side of the plot in Figure 2. However, a more accurate appraisal of the evolution of sensors signals can be acquired calculating, by variance analysis, the probability of class separation as a function of time.

The probability of null hypothesis (p-value) was calculated with data collected at different experimental times from the first second after the beginning of the exposure up to 75 seconds later, immediately before to switch the inlet flow to the technical air background. The p-value has been calculated with the non-parametric Kruskal-Wallis rank sum test.

Figure 4 shows the behaviour of the p-value respect to the exposure time.

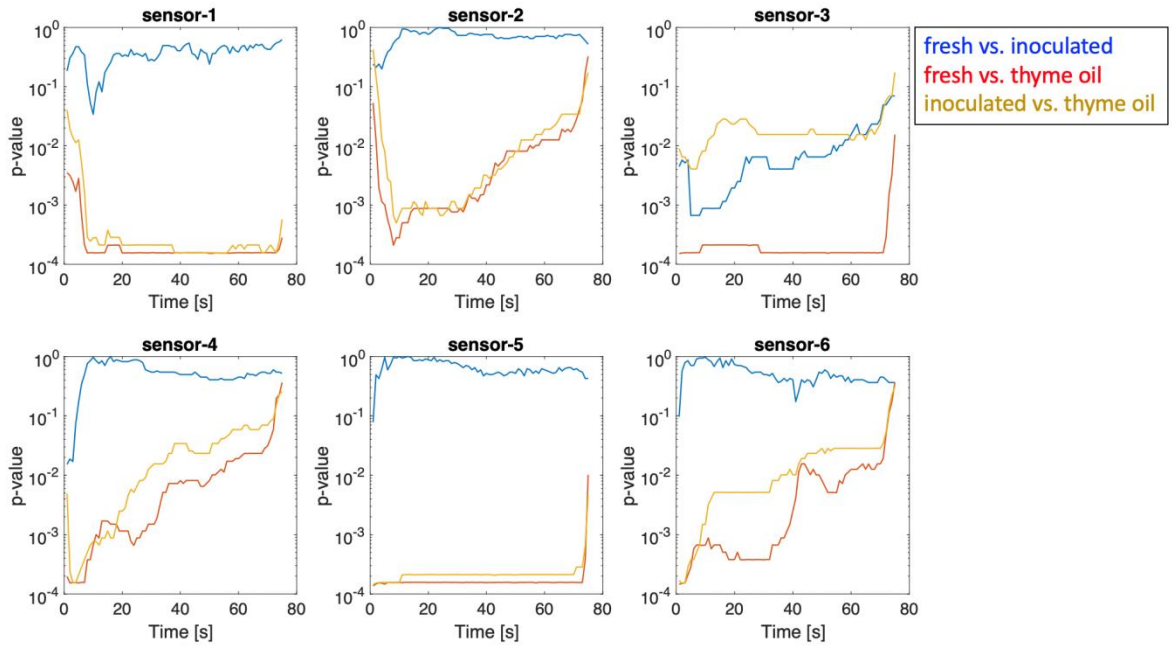

Figure 4: time evolution of the p-value calculated for the mutual separation between classes, for each sensor, as a function of the time from the beginning of exposure.

The analysis of variance shows that, except sensor 3, all sensors separate oil-thyme treated samples respect to the others. Largest difference between classes is captured about 10 s after the beginning of exposure. This behaviour is similar with the concentration evolution of the slowly evaporating compounds plotted at the left side of Figure 2. Thus, it may be interpreted as a clear consequence of the evolution of the headspace during its dynamic extraction. Moreover, the evolution of the differences between classes are also rather variable suggesting that the composition of the headspace also changes during the headspace extraction.

Variance analyses of PTR-ToF-MS mass peaks, similar to those reported for sensors, showed the largest difference between classes in correspondence of the peak of concentration shown in Figure 2. Since the main interest of this study is to compare PTR-ToF-MS signals with those of sensors, the analysis was restricted to the most abundant mass peaks. In particular, 29 mass peaks whose average abundance was above 10 ppb were selected for further analysis. The list of the selected mass peaks is shown in Table 1. Most of these compounds are characterized by a non linear evolution of the PTR-ToF-MS signal, labelled as groups 2, 3 and 4 in figure 2. Few compounds show a progressive increase of the concentration (groups 1 and 6 in fig. 2).

	m/z	**Chemical formula**	**Concentration behaviour (group in fig. 2)**	**Largest abundance [ppbv]**	**Smallest abundance [ppbv]**	**Average abundance [ppbv]**
1	31.018	$CH_2O.H^+$	2	224.78	2.09	162.51
2	34.037	$C^{13}H3OH.H^+$	3	272.25	0.38	196.45
3	39.023	$C_3H_3^+$	2	62.92	1.21	32.52
4	41.039	$C_3H_5^+$	3	338.59	3.45	184.09
5	43.018	$C_2H_3O^+$	3	110.42	4.10	65.84

6	43.029	$CH_2N_2.H^+$	2	111.06	0.72	73.92
7	43.054	C3H7+	3	266.07	1.33	123.69
8	45.990	NO2+??	4	31.67	3.59	16.35
9	46.037	$C^{13}CH_4O.H^+$	2	85.40	1.31	35.52
10	48.053	$C_2H_5O.H^+$	3	202.82	0.40	72.70
11	55.038	$(H_2O)_3.H^+$	6	72.28	37.44	58.55
12	55.054	$C_4H_7^+$	3	41.58	2.66	15.24
13	57.070	$C_4H_9^+$	3	339.48	2.04	146.84
14	59.049	$C_3H_6O.H^+$	2	1186.09	13.36	629.43
15	61.012	$C_2H_4S.H^+$	4	33.86	0.14	17.95
16	61.028	$C_2H_4O_2.H^+$	3	186.63	6.22	97.58
17	64.029	$C^{13}CCH_6S.H^+$	4	256.18	0.10	138.80
18	67.055	$C_5H_7^+$	1	67.45	0.31	15.26
19	71.086	$C_5H_{11}^+$	3	59.06	0.32	18.62
20	73.065	$C_4H_8O.H^+$	2	277.46	0.80	112.65
21	75.044	$C_3H_6O_2.H^+$	2	96.07	0.65	63.00
22	87.081	$C_5H_{10}O.H^+$	2	28.53	0.24	14.26
23	89.060	$C_4H_8O_2.H^+$	3	26.53	0.37	17.57
24	91.056	$C_4H_{10}S.H^+$	1	156.64	0.34	31.70
25	97.029	$C_5H_4O_2.H^+$	1	36.70	0.43	18.41
26	119.086	$C_9H_{11}^+$	1	83.87	0.11	17.74
27	135.116	$C_{10}H_{15}^+$	1	604.84	0.16	119.48
28	138.136	$C_9{}^{13}CH_{17}^+$	1	222.87	0.09	50.01
29	153.128	$C_{10}H_{16}O.H^+$	6	82.01	0.12	20.38

Table 1. List of selected mass peaks whose mean abundance is larger than 10 ppb. The time behaviour of the PTR-ToF-MS signals is attributed to one of the 6 classes shown in figure 2. For each mass smallest and largest abundances are also listed.

Kruskal-Wallis test was performed for each mass peak at each time of measurement. Figure 5 shows the evolution of the p-value with time for each selected mass peak.

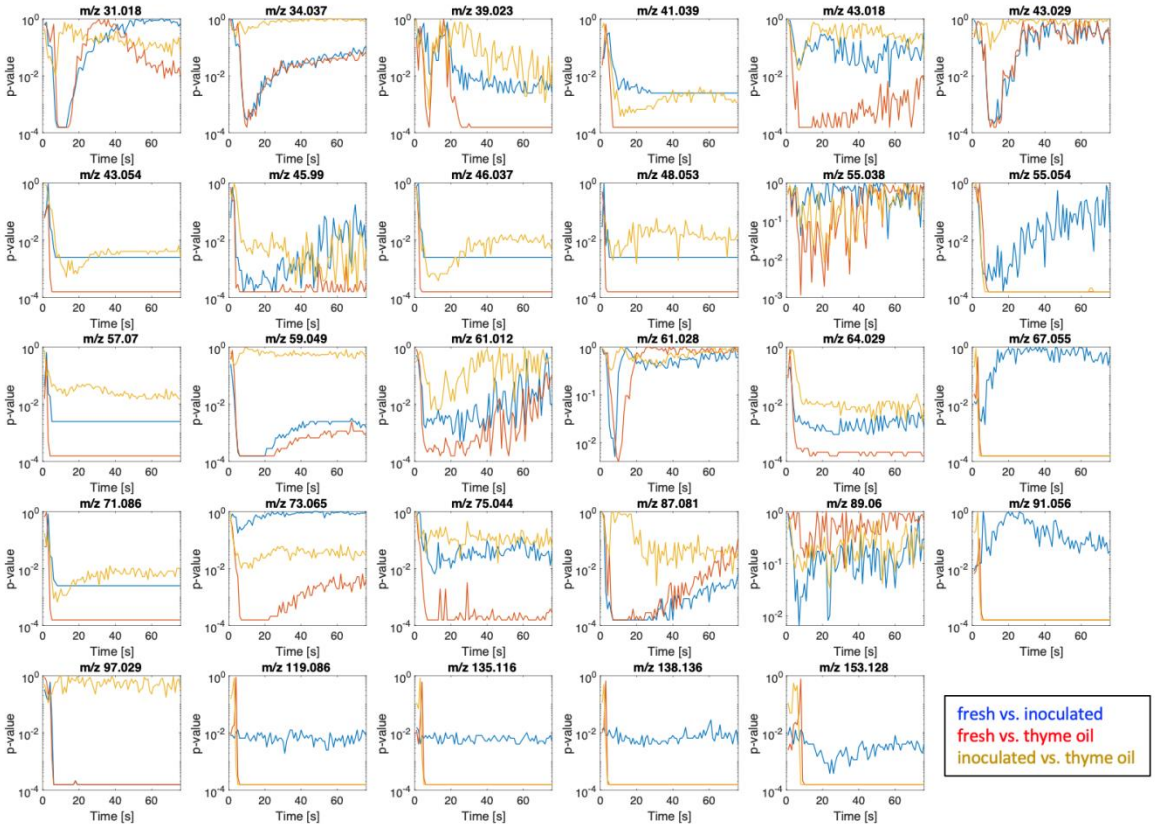

Figure 5: Time evolution of the p-value calculated for the mutual separation between classes and for each PTR-ToF-MS mass peak whose mean abundance is larger than 10 ppb.

It is interesting to observe that different mass peaks showed a different behaviour of p-value. Moreover, for the same mass peak the behaviour of p-values with respect to the separation between different classes may be different too. This result is rather expected considering that each volatile compound is characterized by a proper evaporation rate, and contributes differently to the separation between the classes. In addition, it should be taken into consideration that a PTR-ToF-MS mass peak could consist of different monomers with different physicochemical properties.

The consequences of the headspace variable composition to sensors and PTR-ToF-MS signals can be efficiently studied by multivariate analysis of the datasets. The number of samples does not enable a reliable classification of data, and on the other hand a classifier might also hide the changes occurring along the time. Rather, it is more useful and convenient to study the correlation among variables (either sensors or PTR-ToF-MS mass peaks) and to display the variation of the relationship between data, and Principal Component Analysis (PCA) is an adequate tool for this scope.

Figures 6 and 7 show the plots of the first two principal components calculated with the data of sensors and most abundant PTR-ToF-MS mass peaks. PCA was calculated on standardized data where each variable is normalized to zero mean and unitary variance.

The scores plots of sensors data (Figures 6A and 6B) show that the separation of the three classes achieved at 10 s is almost completely lost at 60 s. This is particularly evident for inoculated and thyme oil treated samples. In contrast, the data of pristine paste are closely clustered even after 60 s. The different effect of time on the three classes suggests that also the qualitative composition of headspace changes during the measurement. A further demonstration is offered by the radically different loadings plots (Figures 6C and 6D). To correctly interpret the loadings plot it is necessary to consider that the sensors signals are negative, thus a larger response means a larger negative signal.

The scores plot at 10 s is dominated by sensors 3, 5, and 2, where each of these sensors points towards a different class. At 60 s the relationship between sensors and classes is almost lost and only sensor 2 retains its correlation with the group of thyme oil treated samples.

Rather than the changes of scores plot, the variations in loadings plots indicate the changes of the headspace composition. Figures 6C and 6D show that for some sensors the relationship between sensors and classes at short and long time changes.

PTR-ToF-MS data scores plots are less affected by the decrease of concentration of VOCs. The scores plots calculated with data taken at after 10 and 60 seconds are indeed rather similar (Figures 7A and 7B). More evident are the changes in the loadings plots (Figures 7C and 7D). At 10 s all masses contribute either to thyme oil treated or to pristine paste samples, except variable 23, corresponding to m/z 89.060 attributed to $C_4H_8O_2.H^+$. At 60 s the role of variable 16 respect to inoculated samples emerges; this variable corresponds to m/z 61.028 whose formula is ($C_2H_4O_2.H^+$).

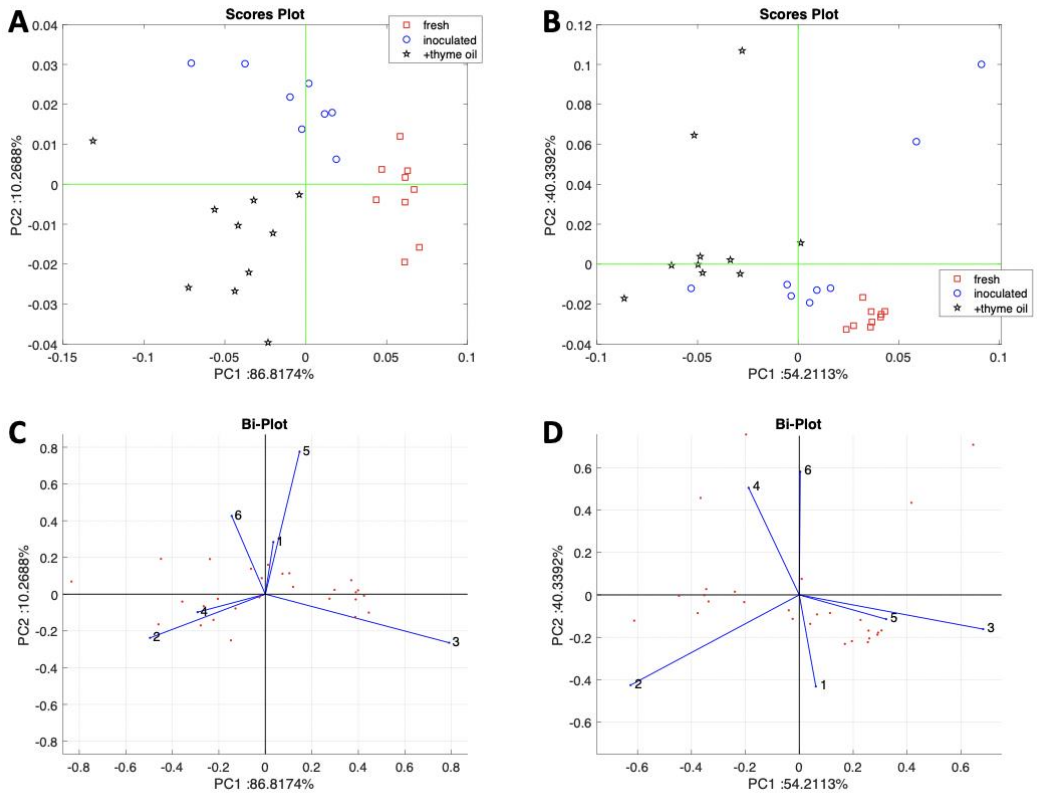

Figure 6: PCA of sensors data. A) scores plot with data at t=10 s; B) scores plot with data at t= 60 s; C) loadings plot with data at t=10 s; D) loadings plot with data at t=60 s.

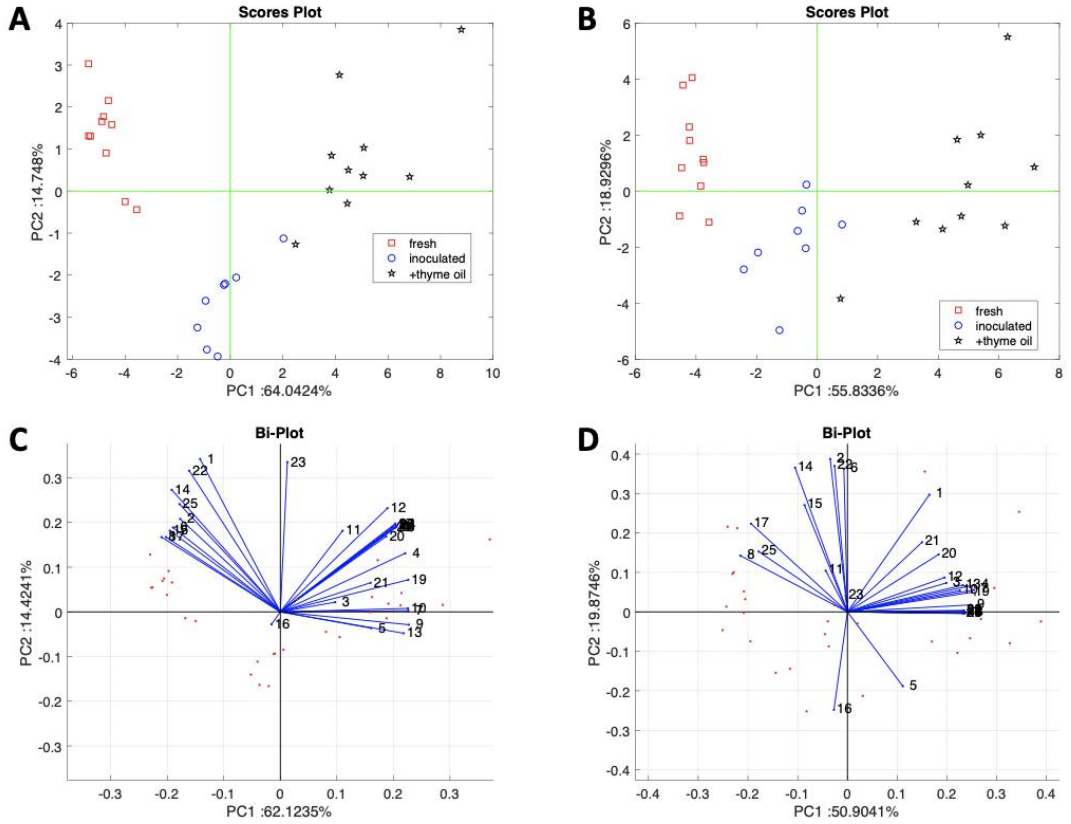

Figure 7: PCA of PTR-ToF-MS data. Analysis has been restricted to those masses whose mean abundance is larger than 10 ppb (Table 1). A) scores plot with data at t=10 s; B) scores plot with data at t= 60 s; C) loadings plot with data at t=10 s; D) loadings plot with data at t=60 s.

Sensors and PTR-ToF-MS data were differently affected by the variation of headspace abundance. The behaviour of sensors data was unexpected because, as shown in figure 3, in spite of the variable headspace composition, sensors signals are characterized by a progressive increase of the amount of absorbed molecules.

This behaviour can be explained considering that the measured samples are characterized by a non-negligible amount of water. Indeed, as typical in many foodstuffs, water is by far the more abundant component of the matrix.

Due to its large concentration in the food matrix, water vapour, instead of decreasing as the other VOCs, steadily increased during the measurement. The relative humidity of the sample was measured by a humidity sensor placed in the sensors cell. Humidity sensors data correlate with the m/z 55.038, that is identified as water cluster and is related to headspace humidity.

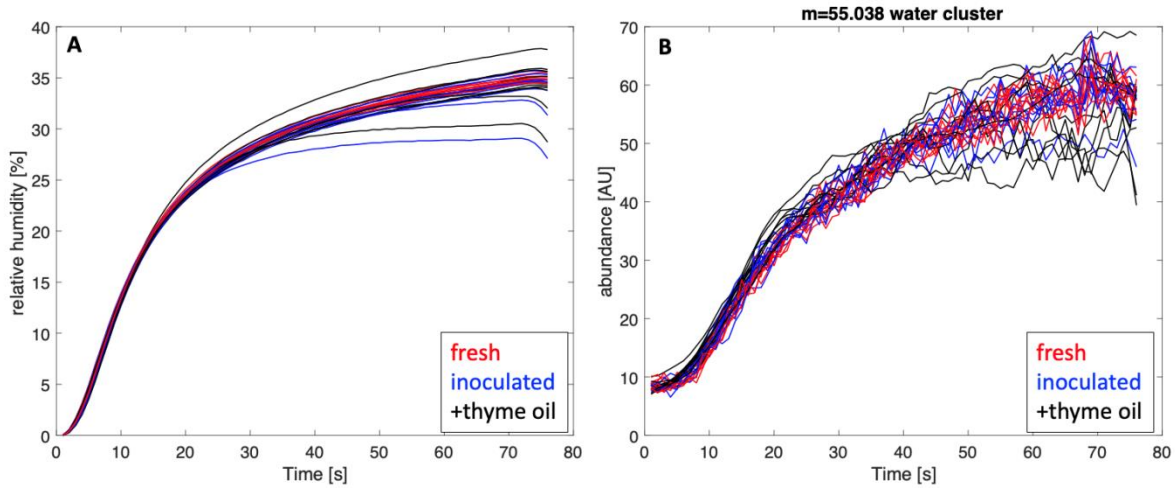

Figure 8: Evolution of relative humidity (panel A) and abundance of m/z 55.038, identified as water cluster (panel B) in all measured samples. Curves are coloured according to their class.

Figure 8 shows the relative humidity as measured by the humidity sensor of the electronic nose (Figure 8A) and the abundance of m/z 55.038 measured by PTR-ToF-MS (Figure 8B). The two signals are obviously proportional to each other: the linear correlation coefficient between the two sets is larger than 0.99. No relationship between the humidity of the sample and any class was found in Figure 8. The absence of relationship between humidity and classes is also visible in Figure 5, where m/z 55.038 is a variable with the largest p-value and that in practice does not discriminate the different classes.

Even if the sensitivity to water, in terms of Hz/ppm, may be small respect to that towards other VOCs, the actual concentration of water can well exceed that of VOCs. In these samples the contribution of water in the sensors signal is not negligible and after the peak of VOCs concentration, sensors surface continues to accumulate water molecules and the sensor signal keeps increasing.

Eventually, the analysis of variance at different times provides a valid methodology to determine the optimal measurement time respect to the subtraction of relative humidity contribution which requires a long exposure of sensors. Short exposures, besides maximizing the information content of sensor signals, also reduce the burden of unwanted absorbed water molecules that could also induce drift effects in sensor signals.

Conclusions

In gas sensors it is common opinion that optimal sensor response is obtained when the sensor signal reaches a steady value. In this paper it has been shown that although the sensor signal progressively increases during the exposure to the sample, the information content of the signal itself, here represented by classes separation, may decrease. Thus, the behaviour of sensor signals is not always completely representative of the phenomena underlying the sensor response. This behaviour may be simply explained by the fact that these sensors are sensitive to volatile compounds and to humidity. In high humidity samples, such as many food products, the concentration of water vapour may continuously grow during head-space extraction while volatile compounds, a

minor component in the sample, quickly reach a maximum concentration and possibly decrease if sampled from a finite volume.

Taking advantage of the on-line connection of gas sensors and PTR-ToF-MS, the sensor response has been directly compared with the sample composition at the same time. An electric equivalent circuit of the dynamic headspace sampling has been introduced. VOCs concentration in sensors and detector cells follows different evolutions depending on the evaporation rate of the volatile compounds.

For most of the compounds, the concentration at which the sensors are exposed shows a peak a few seconds after the beginning of the measurement. It has been shown here that the sensor response at the time of maximum concentration corresponds to the largest information content, allowing for a clear separation of the three classes.

Among the compounds whose concentration in the sensor cells is monotonically growing we found humidity. Thus a simple explanation of sensor response has been provided where sensor are considered sensitive to the total volatile compounds and the relative humidity.

Eventually, this study suggests that in electronic nose experiments an optimal measurement time may exist at which the information content of sensors signals is largest. If the sample is not homogeneous but it includes compounds with different evaporation enthalpies, the optimal time may be, in principle, different for each class.

The use of a PTR-ToF-MS in series with gas-sensor cells is a valuable tool to better understand and support the optimisation of gas-sensors arrays. Because of cost and size, it is obviously not an alternative to gas sensors. However, photoionization detectors (PIDs) which are fast, sensitive and non-selective can efficiently complement gas sensors applications by providing the information about the time evolution of total VOCs and thus the time at which the sensor signal could be most informative and reliable. Recent improvements in PID design are expected to result in low-cost miniaturized devices that could be easily implemented in gas sensor arrays [17].

References

[1] K. Burlachenko, J.; Kruglenko, I.; Snopok, B.; Persaud, Sample handling for electronic nose technology: State of the art and future trends, TrAC - Trends Anal. Chem. 82 (2016) 222–236.

[2] N.H. Snow, G.C. Slack, Head-space analysis in modern gas chromatography, TrAC - Trends Anal. Chem. 21 (2002) 608–617. https://doi.org/10.1016/S0165-9936(02)00802-6.

[3] B. Kolb, L.S. Ettre, Static Headspace-Gas Chromatography: Theory and Practice, Second Edition, 2006. https://doi.org/10.1002/0471914584.

[4] D.A. Storace, L.B. Cohen, Measuring the olfactory bulb input-output transformation reveals a contribution to the perception of odorant concentration invariance, Nat. Commun. 8 (2017). https://doi.org/10.1038/s41467-017-00036-2.

[5] B. Salehi, A.P. Mishra, I. Shukla, M. Sharifi-Rad, M.D.M. Contreras, A. Segura-Carretero, H. Fathi, N.N. Nasrabadi, F. Kobarfard, J. Sharifi-Rad, Thymol, thyme, and other plant sources: Health and potential uses, Phyther. Res. 32 (2018) 1688–1706. https://doi.org/10.1002/ptr.6109.

[6] F.D. Gonelimali, J. Lin, W. Miao, J. Xuan, F. Charles, M. Chen, S.R. Hatab, Antimicrobial properties and mechanism of action of some plant extracts against food pathogens and spoilage microorganisms,

Front. Microbiol. 9 (2018). https://doi.org/10.3389/fmicb.2018.01639.

[7] R. Paolesse, S. Nardis, D. Monti, M. Stefanelli, C. Di Natale, Porphyrinoids for Chemical Sensor Applications, Chem. Rev. 117 (2017). https://doi.org/10.1021/acs.chemrev.6b00361.

[8] R.S. Blake, P.S. Monks, A.M. Ellis, Proton-transfer reaction mass spectrometry, Chem. Rev. 109 (2009) 861–896. https://doi.org/10.1021/cr800364q.

[9] R. Capuano, I. Khomenko, F. Grasso, V. Messina, A. Olivieri, L. Cappellin, R. Paolesse, A. Catini, M. Ponzi, F. Biasioli, F. Biasioli, C. Di Natale, Simultaneous Proton Transfer Reaction-Mass Spectrometry and electronic nose study of the volatile compounds released by Plasmodium falciparum infected red blood cells in vitro, Sci. Rep. 9 (2019). https://doi.org/10.1038/s41598-019-48732-x.

[10] A. D'Amico, C. Di Natale, C. Falconi, G. Pennazza, M. Santonico, I. Lundstrom, Equivalent electric circuits for chemical sensors in the Langmuir regime, Sensors Actuators, B Chem. 238 (2017) 214–220. https://doi.org/10.1016/j.snb.2016.07.011.

[11] P.A. Brown, S.M. Cristescu, S.J. Mullock, D.F. Reich, C.S. Lamont-Smith, F.J.M. Harren, Implementation and characterization of an RF ion funnel ion guide as a proton transfer reaction chamber, Int. J. Mass Spectrom. 414 (2017) 31–38. https://doi.org/10.1016/j.ijms.2017.01.001.

[12] U. Oprea, A.; Weimar, Gas sensors based on mass-sensitive transducers part 1: transducers and receptors—basic understanding, Anal. Bioanal. Chem. 411 (2019) 1761–1787.

[13] J.W. Buchler, Synthesis and properties of metalloporphyrins, in: D. Dolphin (Ed.), Porphyrins Vol. 1, Academic Press, 1978.

[14] L. Cappellin, F. Biasioli, A. Fabris, E. Schuhfried, C. Soukoulis, T.D. Märk, F. Gasperi, Improved mass accuracy in PTR-TOF-MS: Another step towards better compound identification in PTR-MS, Int. J. Mass Spectrom. 290 (2010) 60–63. https://doi.org/10.1016/j.ijms.2009.11.007.

[15] L. Cappellin, F. Biasioli, E. Schuhfried, C. Soukoulis, T.D. Mark, F. Gasperi, Extending the dynamic range of proton transfer reaction time-of-flight mass spectrometers by a novel dead time correction, Rapid Commun. Mass Spectrom. 25 (2011) 179–183. https://doi.org/10.1002/rcm.4819.

[16] W. Lindinger, A. Hansel, A. Jordan, On-line monitoring of volatile organic compounds at pptv levels by means of Proton-Transfer-Reaction Mass Spectrometry (PTR-MS) Medical applications, food control and environmental research, Int. J. Mass Spectrom. Ion Process. 173 (1998) 191–241. https://doi.org/10.1016/s0168-1176(97)00281-4.

[17] S. Pyo, K. Lee, T. Noh, E. Jo, J. Kim, Sensitivity enhancement in photoionization detector using microelectrodes with integrated 1D nanostructures, Sensors Actuators, B Chem. 288 (2019) 618–624. https://doi.org/10.1016/j.snb.2019.03.045.